PCCP

Accepted Manuscript

ROYAL SOCIETY OF CHEMISTRY

www.rsc.org/pccp

Journal Name

ARTICLE TYPE

Cite this: DOI: 10.1039/xxxxxxxxxx

On the energetics of cation ordering in tungsten-bronze-type oxides†

Gerhard Henning Olsen, Sverre Magnus Selbach, and Tor Grande*

Received Date
Accepted Date

DOI: 10.1039/xxxxxxxxxx

www.rsc.org/journalname

Oxides with the tetragonal tungsten bronze (TTB) structure are well-known ferroelectrics that show a large flexibility both with respect to chemical composition and cation ordering. Two of the simplest compounds in this family are lead metaniobate ($PbNb_2O_6$ or PN) and strontium barium niobate ($Sr_xBa_{1-x}Nb_2O_6$ or SBN). While PN is a classical ferroelectric, SBN goes from ferroelectric to relaxor-like with increasing Sr content, with a polar direction different from that in PN. The partially occupied sublattices in both systems give the possibility for cation order–disorder phenomena, but it is not known if or how this influences the polarization and ferroelectricity. Here, we use density functional theory (DFT) calculations to investigate how cation and cation vacancy ordering influences the energetics of these compounds, by comparing both the energy differences and the barriers for transition between different cation configurations. We extend the thermodynamic model of O'Neill and Navrotsky, originally developed for cation interchange in spinels, to describe the order–disorder phenomenology in TTB oxides. The influence of order–disorder processes on the functional properties of PN and SBN is discussed.

1 Introduction

In the family of ferroelectric oxides based on $BO_{6/2}$ octahedra, oxides with the tetragonal tungsten bronze (TTB) structure form the second largest group after the perovskites.[1] The simplest of these compounds is lead metaniobate, $PbNb_2O_6$ or PN, which has a high Curie temperature of 570 °C.[2] It is, however, only stable at temperatures above 1200–1250 °C, and metastable with respect to a rhombohedral polymorph below this temperature range.[3–5] A lead-free analogue to PN is strontium barium niobate, $Sr_xBa_{1-x}Nb_2O_6$ or SBN, which is apparently stable in the TTB structure down to ambient temperature, although with a lower T_C of 70–200 °C, depending on composition.[6,7]

Both PN and SBN have the general formula $(A1)_2(A2)_4C_4(B1)_2(B2)_8O_{30}$, with five formula units in the unit cell, and space group symmetry $P4/mbm$ in the aristotype structure. The A1 and A2 sites form, respectively, pentagonal and square channels that run parallel to the tetragonal axis, and which accomodate the Pb^{2+}, Sr^{2+} and Ba^{2+} cations. The C sites form narrow triangular channels, and are usually vacant, as only a few cations such as Li^+ and Nb^{5+} are small enough for these sites.[8,9] The B1 and B2 sites are symmetrically different octahedral positions, and are fully occupied by Nb^{5+} in both PN and SBN. With all A-site cations divalent and Nb in the pentavalent state, as is the case in PN and SBN, charge neutrality requires that 5 out of 6 A-sites be occupied.

While PN and SBN are similar in terms of structure, there are fundamental differences in the behaviour of the two compounds. PN is a classical ferroelectric, while SBN is ferroelectric for barium-rich compositions, but becomes relaxor-like for strontium contents higher than approximately $x = 0.6$.[10] The ferroelectric transitions are also different in terms of symmetry: While SBN remains tetragonal at all temperatures, with a spontaneous polarization in the [001] direction below T_C,[6] PN has an in-plane polarization along the [110] direction referred to the aristotype cell, leading to an orthorhombic distortion in the ferroelectric state.[11] The explanation of this difference, or indeed the mechanism for ferroelectricity in general, is not fully understood for these compounds. It has been suggested that in the ferroelectric state, the main contribution to the polarization is displacement of Nb^{5+} along [001] for SBN, and in-plane displacement of the A-site cations for PN.[12] This difference could be related to the stereochemically active $6s^2$ lone pair on Pb^{2+}, in analogy with the perovskite titanates of lead and barium.[13] Nevertheless, the picture is less clear for TTB's, due to the significantly more complicated structure.

In addition to the complexity of the crystal structure itself, the partial occupancies in the tungsten-bronze oxides give rise to the possibility of cation order–disorder phenomena. Non-convergent

Department of Materials Science and Engineering, Norwegian University of Science and Technology (NTNU), NO-7491 Trondheim, Norway. Tel: +47 735 94084. E-mail: tor.grande@ntnu.no

† Electronic Supplementary Information (ESI) available: Derivation of thermodynamic equations, energetics data in tabular form and data on crystal structures. See DOI: 10.1039/b000000x/

ordering is well known in spinels with AB_2O_4 stoichiometry, but has to our knowledge never been addressed for materials with the TTB-type crystal structure. In spinels, the cation exchange between the tetrahedral and octahedral sublattices can be thought of as a chemical reaction,[14] and the cation distribution can thus be modelled as a simple chemical equilibrium.[15–17] The tungsten-bronzes are similar to the spinels in terms of cation distribution between two non-equivalent sublattices, so a similar hypothesis should also apply here. Intuitively, the larger ionic radius of Ba^{2+} relative to Sr^{2+} and Pb^{2+} implies that the former will preferentially occupy the larger pentagonal sites, which has also been found experimentally.[6,18] However, even this simple effect of atomic size is not obvious: Large cations preferentially occupy the larger octahedral sites in 4–2 spinels, while the opposite is actually true for 2–3 spinels.[16] There is therefore no guarantee that a simple argument based on atomic size also holds for a different crystal structure such as the TTB-type.

In this study, we examine the differences between the tungsten-bronze-type oxides PN and SBN by density functional theory (DFT) calculations. Particular attention is given to the effect of cation ordering between the A1 and A2 sites, and the effect of this on energetic stability. This line of thinking has previously been applied to perovskite relaxors,[19,20] but no first-principles study of cation ordering in TTB materials has to our knowledge been done.In our work, we seek to study the energetics of order–disorder effects in the paraelectric state of the materials, where sufficient cation mobility may occur only during synthesis far above T_C. The influence of cation ordering on polarization and lattice instabilities due to ferroelectric order is not included in this study, but will be followed up in future work. For computational treatment of these effects, we employ a supercell approach which makes it possible to sample several different cation configurations. We analyze the energy landscape between the configurations, consider the plausibility of cation ordering in tungsten-bronze-type oxides, and discuss possible reasons for the relaxor properties of strontium-rich compounds in the SBN system.

2 Methodology

2.1 Combinatorial aspects

An analysis is made of the different orderings possible in ANb_2O_6-type tungsten-bronzes. Starting with a single unit cell containing 45 atoms (5 formula units of ANb_2O_6), there are 6 sites among which to distribute 5 cations (or, equivalently and more convenient, six sites among which to distribute 1 vacancy). The four pentagonal (P) sites are equivalent, as are also the two square (S) sites (see Figure 1a), so for a single unit cell, there are only two unique configurations.

A more realistic approach is to look at the possible configurations in a 1x1x2 *supercell*, by doubling the unit cell in the c direction. In such a cell, there are a total of 12 A-sites (pentagonal and square), as shown in Figure 1b. Among these 12 sites, there are 10 atoms and 2 vacancies to be distributed. For the rest of this discussion we focus on distribution of the vacancies, and count and name the configurations according to the following scheme:

- The two vacancies can be distributed between square and pentagonal sites in three ways: Both pentagonal (PP), both square (SS), or one of each (SP).
- If the first vacancy is located on a square site, there are three possible ways to place the second vacancy on another square site: On the other square site in the same layer; diagonally in the layer above; or directly above the first. Hence, there are three SS configurations.
- If the first vacancy is located on a pentagonal site, there are five possible ways to place the second vacancy on another pentagonal site: Two in the same layer (next to the first or diagonally opposite from it); the same two positions in the layer above; or directly above the first. Hence, there are five PP configurations.
- If the first vacancy is located on a square site and the second on a pentagonal, they can either be in the same layer, or in different layers. Hence, there are two SP configurations.
- We use a triplet [hkl] to describe the (approximate) vector between the two vacancies. For example, two pentagonal vacancies within the same layer can be designated as PP[100] or PP[110] configurations, depending on whether the vacancies are "nearest neighbours" within the unit cell, or diagonally opposite from each other, respectively.

This scheme leads to a total of 10 unique configurations for each composition. These are summarized in Table 1, which gives the systematic name for each configuration, and the local space group symmetry arising from the cation ordering.[22] As the table shows, the five PP configurations lead to local orthorhombic space group symmetries, the three SS configurations preserve the tetragonal symmetry (with SS[110] even preserving the aristotype space group $P4/mbm$), and the two SP configurations lead to local monoclinic symmetry. The 10 configurations for a 1x1x2 supercell also include the two configurations possible for a single unit cell: PP[001] is identical to a single unit cell with the vacancy on a pentagonal site, while SS[001] is identical to a single unit cell with the vacancy on a square site.

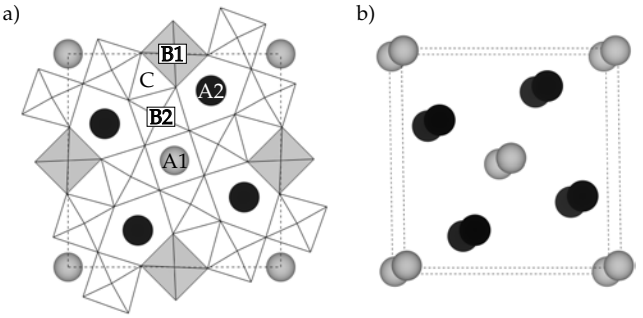

Fig. 1 a) Projection along the c axis of the tetragonal tungsten-bronze unit cell in the $P4/mbm$ aristotype, with labels for the different cation sites. The A1 and A2 sites are represented by grey and black spheres, respectively, while the B1 and B2 sites are shown as grey and white octahedra. b) Supercell with a doubled c axis, showing only the A1 and A2 sites with the same colors as in panel a. Figures created with the aid of VESTA.[21]

Table 1 The 10 cation configurations possible for the 1x1x2 supercell considered in this work, showing the systematic name, local space group symmetry, and a sketch of the configuration (cations represented by grey spheres, vacant sites white)

PP[100]	PP[110]	PP[101]	PP[111]	PP[001]
$Pmc2_1$	$Cmmm$	$Pmn2_1$	$Cmcm$	$Amm2$
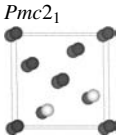	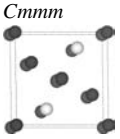	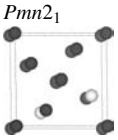	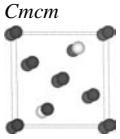	
SS[110]	**SS[111]**	**SS[001]**	**SP[110]**	**SP[111]**
$P4/mbm$	$P4/mcn$	$P4/m$	Pm	Pm
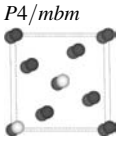	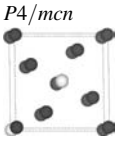	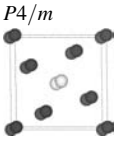		

In principle it is possible to extend the investigation to even larger supercells, such as 1x1x3 or 1x1x4, but this was not performed. Possible effects of increasing the supercell size is included in the discussion.

2.2 Thermodynamic model

To gain insight into the possibility of cation ordering, we extend the thermodynamic model of O'Neill and Navrotsky[16] for the cation distribution in spinels. The fundamental assumption, introduced by Schmalzried[14] and elaborated by Navrotsky and Kleppa,[15] is that the interchange of cations between two distinct sublattices can be viewed as a chemical equilibrium:

$$[Av](A_4)\mathrm{Nb}_{10}\mathrm{O}_{30} \rightleftharpoons [A_{1+x}v_{1-x}](A_{4-x}v_x)\mathrm{Nb}_{10}\mathrm{O}_{30}, \qquad (1)$$

where $[A]$ denotes a cation A on an A1 or square site, (A) denotes a cation A on an A2 or pentagonal site, and v denotes a cation vacancy. This also introduces an interchange parameter, x, which ranges from 0 (all vacancies on square sites, i.e., SS configurations) to 1 (all vacancies on pentagonal sites, i.e., PP configurations). It is then assumed that the free energy of the cation interchange reaction (1) can be expressed as

$$\Delta G_{\mathrm{int}}(x) = \alpha x + \beta x^2 + RT\sum_s b_s \sum_i x_{i,s} \ln x_{i,s}, \qquad (2)$$

where the last term on the right side is the entropy of mixing for an ideal solution, with $x_{i,s}$ being the fractional occupancy of species i on site s, and b_s the multiplicity of site s. This is a purely configurational entropy contribution, *i.e.* it is assumed that all other entropy changes following reaction (1) are negligible. The enthalpy consists of two terms, one linear and one quadratic in the interchange parameter x, as was proposed by O'Neill and Navrotsky[16] as an expansion of the original model by Navrotsky and Kleppa.[15] Effects of volume and non-configurational entropy are neglected. The energy difference between different configurations with the same degree of cation interchange is not taken into account at this stage, so all SS configurations are for now assumed to be degenerate, and the same applies for the PP and SP configurations. A simple differentiation of the entropy part shows that maximal configurational entropy is obtained for $x = 2/3$. This is analogous to AB_2O_4 spinels, which also have a maximal configurational entropy for $x = 2/3$ when x is the fraction of B cations on tetrahedral sites (this is referred to as a random spinel).

By writing out (2) for the TTB structure (see ESI† for details), and differentiating with respect to x, the following expression is found for equilibrium conditions:

$$\ln K = \ln \frac{x(1+x)}{(1-x)(4-x)} = -\frac{\alpha + 2\beta x}{RT}, \qquad (3)$$

where K can be recognized as the equilibrium constant for the simplified cation exchange reaction $[v] + (\mathrm{A}) \rightleftharpoons (v) + [\mathrm{A}]$, using the same notation as in (1). Equation (3) gives the relation between temperature and degree of inversion once the enthalpy coefficients α and β are determined. This can be done experimentally by determining x from refinement of diffraction data at different T, although it could be challenging to obtain high-quality data at temperatures high enough for the cation mobility to be appreciable. Here, we will instead estimate the parameters by calculating the enthalpy term in (2) from first principles for cation configurations with different x.

2.3 Computational details

A non-polar SBN unit cell was created by starting from structural data from literature[18] and searching for pseudosymmetry[23] in the non-polar space group $P4/mbm$ (127). The end members of the SBN system, $SrNb_2O_6$ (SN) and $BaNb_2O_6$ (BN), were modelled by replacing all Sr and Ba in the unit cell with only one of the two elements, and setting the lattice parameters a and c to the values extrapolated from the polynomial expressions given by Podlozhenov *et al.*[18] For PN, lattice parameters from Labbé[12] were used, after extracting the pseudosymmetric $P4/mbm$ structure from the experimental space group $Amm2$ as described above.

Total energies were obtained by density functional theory (DFT) calculations with the VASP code,[24–27] where the exchange-correlation energy was calculated with the gradient-corrected PBEsol functional.[28] Core electrons were described by the projector-augmented wave (PAW) method,[29,30] with pseudopotentials treating 10 valence electrons for Sr ($4s^24p^65s^2$) and Ba ($5s^25p^66s^2$), 14 for Pb ($5d^{10}6s^26p^2$), 13 for Nb ($4s^24p^64d^35s^2$) and 6 for O ($2s^22p^4$). Valence electrons were described by wave functions expanded in plane waves up to an energy cutoff of 550 eV, which gave well converged lattice parameters in test calculations. Brillouin-zone integration was done on a 2x2x6 Monkhorst-Pack mesh[31] for the 45-atom TTB unit cell, and reduced to a 2x2x3 mesh for the 90-atom supercells. Atomic positions and lattice vectors were relaxed until the forces on the ions were less than 0.01 eV Å^{-1}.

For estimation of the energy barrier between differently ordered configurations, we performed climbing-image nudged elastic band calculations.[32,33] For each composition, we considered two diffusion paths: Between the configurations PP[100] and PP[101]; and between SS[110] and SS[111]. Both consist of a single cation diffusing from one layer to another inside the pentagonal and square tunnels, respectively. The minimum energy

paths (MEPs) were found by considering 3 intermediate images between the endpoints, and optimizing atomic positions until the forces on the ions were less than $0.05\,\mathrm{eV\,\AA^{-1}}$.

3 Results

3.1 Energy landscape of cation configurations

We have calculated the total energy of BN, SN and PN in all 10 configurations considered above, and the results are shown in Figure 2. Both the energy of the initial structures, and the energy

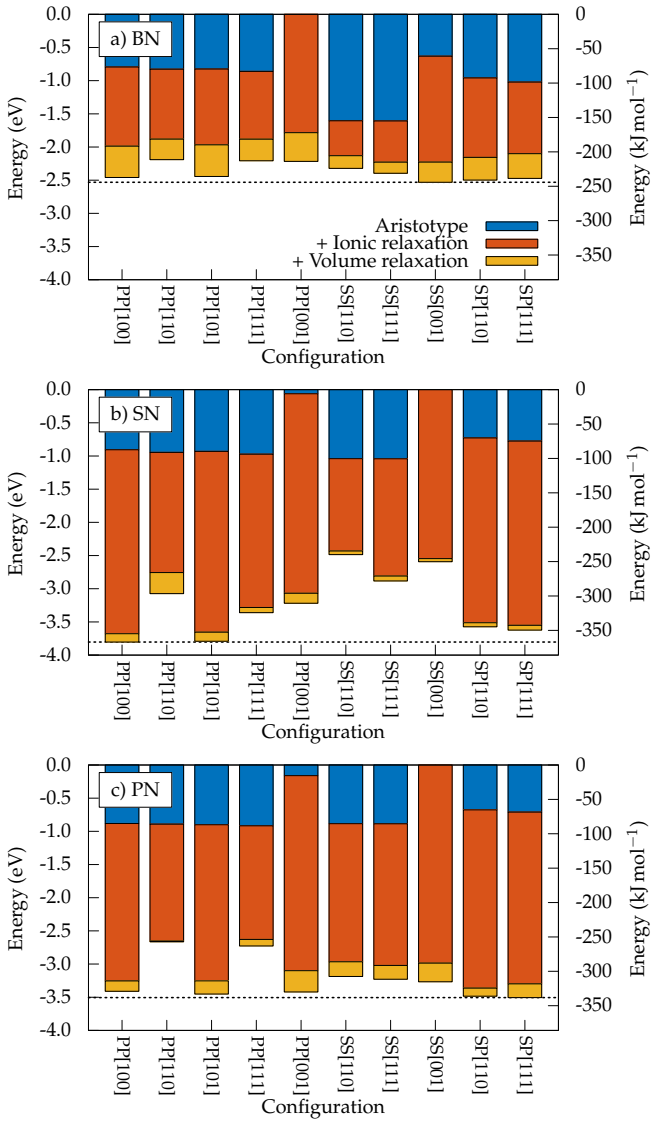

Fig. 2 Relative energy per unit cell ($A_5B_{10}O_{30}$) of the different configurations for a) BN, b) SN and c) PN. The blue bars labeled "Aristotype" show the energies of the intial structures, with space group symmetry as described in Table 1. The red and yellow bars show the additional energy contribution from relaxation of ionic positions and unit cell volume, respectively. The zero level is set at the highest initial energy for each composition (configurations PP[001] or SS[001]).

after optimisation of ionic positions and lattice parameters, are shown. The two configurations that correspond to a single unit cell, PP[001] and SS[001], are the least energetically favourable among the initial structures, and for all three compounds, it is one of these two configurations that has the highest energy initially. The relative energies of the configurations change, however, when ionic relaxation is taken into account. Especially for BN, the initial configurations of highest energy are the ones that gain most by relaxation, giving an overall energy landscape which is quite flat. Subsequent relaxation of the unit cell volume and change of lattice parameters does not contribute as much, as the main energy gain lies in the relaxation of the ionic positions.

For SN and PN, the energy landscape is not quite as flat as for BN, although for both compounds there are several configurations that are very close in energy. The effect of volume relaxation is even lower for SN and PN than for BN, contributing very little to the total energy gain upon optimization of the structure. The effect of ionic relaxation is significant, making the total energy gain larger, at the most around 3.8 eV. The energy for the fully relaxed structures is summarized in Figure 3a, where dashed lines mark the range of energies for each composition. In general, there is no single configuration, or a few configurations, that stand out as significantly more plausible than the others for any of the three compounds.

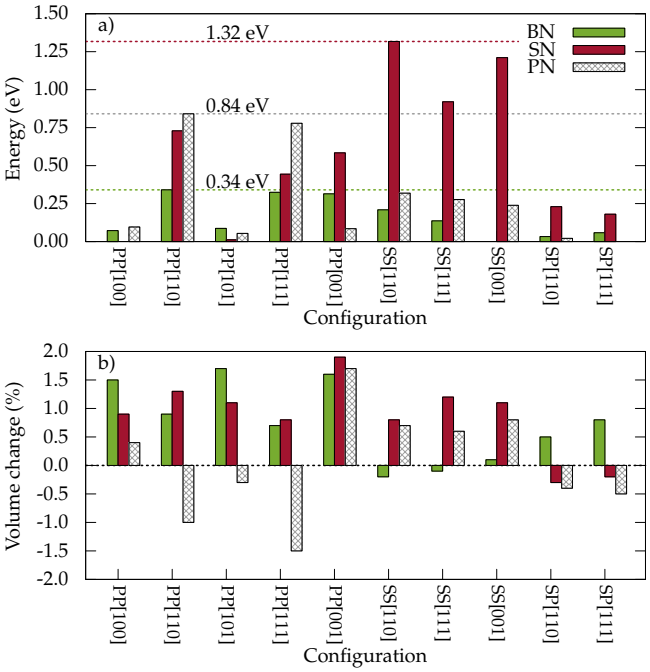

Fig. 3 a) Relative energy per unit cell ($A_5B_{10}O_{30}$) of the fully relaxed structures, corresponding to the total energy shown in Figure 2. The lowest-energy structure is used as reference state for each compound (SS[001] for BN, PP[100] for SN and SP[111] for PN). Dashed lines mark the highest-energy configuration for each composition. b) Volume change corresponding to the relaxed structures in panel a, showing the difference in unit cell expansion associated with different cation configurations.

The change in the unit cell volume following the relaxation of lattice parameters is shown in Figure 3b. The volume change is positive in almost all cases, and as large as up to 4 % with respect to the inital volumes. Some trends are evident: For BN, the expansion is largest for the PP configurations, where Ba^{2+} completely occupies the narrow square channels, and smaller and

slightly negative for the SS configurations. This is as expected, as the large Ba^{2+} cations preferentially occupy pentagonal sites, and will expand the lattice if forced into the smaller square sites. A closer inspection of the lattice parameters shows that the volume change for BN comes from an expansion of the a and b parameters, and a contraction of c with respect to the initial values. Also for SN and PN, the a and b parameters mostly expand (the sole exception being PP[110] for PN, where they slightly contract), while the c parameter either expands or contracts.

3.2 Transition barriers between cation configurations

Due to the similarity in energetic stability between the different configurations, we calculated the energy barriers for transitions between some of these configurations in order to get an impression of how the configurations compare also kinetically. Two cases were considered, namely diffusion of A^{2+} cations in the two different types of channels in the structure. To visualize these cases, the unit cell is shown again in Figure 4a (left panel) together with an alternative view emphasizing the pentagonal and square channels (right panel). Figure 4b shows a perspective view of the channel shapes, with grey and black arrows showing the diffusion paths through the square and pentagonal channels, respectively. Figure 4c shows the minimum energy path (MEP) for these two diffusion processes, where the end configurations are the PP[100] and PP[101] configurations for the pentagonal channel case, and SS[110] and SS[111] for the square channel case. As expected, the energy maximum midway along the path is higher for the square channel than for the pentagonal channel, as the square channels are narrower. In Figure 4d, the height of the energy barriers are compared for the two cases in all three compositions, and the larger size of Ba^{2+} relative to Sr^{2+} and Pb^{2+} is again manifested in the increased transition barrier. The height of the barriers is significant, and dominates over the energy differences between the start and end points, as demonstrated in Figure 4a.

3.3 Application of the thermodynamic model

As stated above, the thermodynamic model we emply here does not take into consideration the energetic differences between configurations with the same value of the cation interchange parameter x. In an attempt to meet this problem, we fitted the enthalpic part of Equation (2) to Boltzmann averages of the energies for each x:

$$\langle E \rangle(T) = \frac{\sum_n E_n e^{-E_n/k_B T}}{\sum_n e^{-E_n/k_B T}}, \qquad (4)$$

where E_n is the energy of configuration n, and the sums are over configurations with the same value of x (i.e., the PP, SS and SP configurations are averaged separately). In this way, at zero kelvin the energies are identical to the single lowest energy for each x, while at finite temperatures there is also a contribution to the energy from population of configurations with higher energy.

Fitting the energies of the fully relaxed structures to Equation (2) as described above leads to the plot shown in Figure 5a. As is evident from this plot, the energies for each x spread out significantly, especially for the PP cases ($x = 1.0$), as was also seen in Figure 3a. Fits to Equation (2) for $T = 0\,\mathrm{K}$ and $T = 1800\,\mathrm{K}$ are

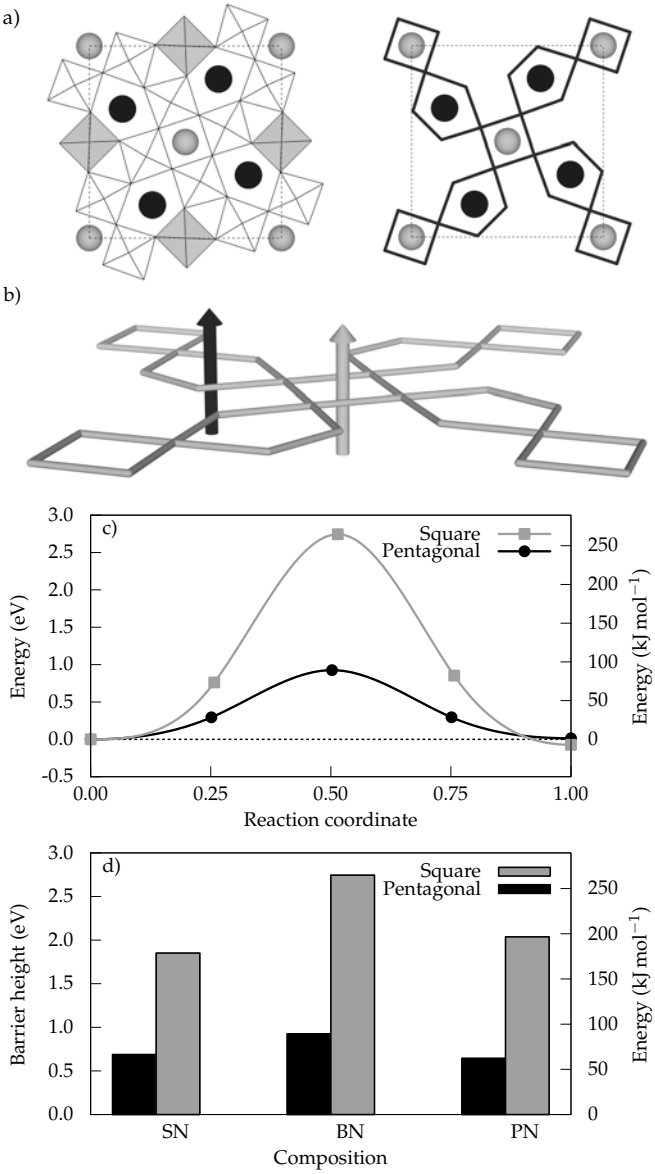

Fig. 4 a) Projection of TTB unit cell along c (left), highlighting the shape of the channels considered for diffusion (right). b) Perspective view of diffusion paths through the square (grey arrow) and pentagonal (black arrow) channels. c) Minimum energy paths (MEP) for cation diffusion through square and pentagonal channels in BN. The square channel diffusion is represented by the transition SS[110] to SS[111], while the pentagonal channel is represented by PP[100] to PP[101]. The dashed line marks the energy of the initial configuration in the diffusion process. d) Comparison of the barrier heights for the MEPs for all three compositions.

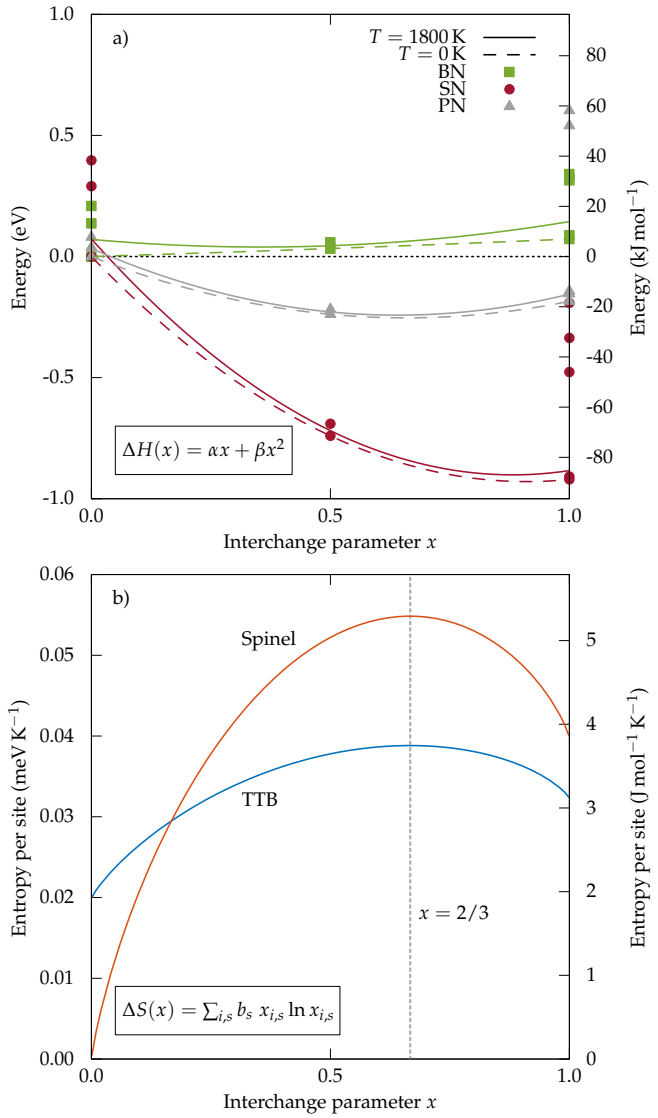

Fig. 5 a) Calculated total energies (points) plotted against the interchange parameter x as defined in reaction (1). $x = 0$ corresponds to the three SS configurations, $x = 0.5$ to the two SP, and $x = 1$ to the five PP configurations. The energy is given in eV per unit cell, corresponding to reaction (1), with the lowest energy configuration at $x = 0$ used as reference. Lines show fits to the enthalpic part of Equation (2), where dashed lines represent zero temperature (only the lowest energy for each x is used) and dashed lines represent $T = 1800\,\mathrm{K}$ through a Boltzmann average of the energies for each x. b) Configurational entropy as a function of the degree of inversion for the TTB structure considered in this work, compared to the configurational entropy of a simple spinel. Values are normalized per site (three for spinel and six for TTB), to make it possible to compare the entropy between two structures with different stoichiometry. In both structures, maximal configurational entropy occurs at $x = 2/3$.

both shown in Figure 5a, in order to get an impression of how much the higher-energy configurations contribute for each x at finite temperatures. In general, this contribution is small, and α and β show very little variation with temperature.

The entropic part of (2) is purely configurational, and is shown in Figure 5b. For comparison, the configurational entropy of a simple spinel is also given, and both are normalized with respect to the number of sites in the structure. It is noteworthy that both the spinel and the tungsten-bronze-type structure show a maximal configurational entropy for $x = 2/3$ with the definitions of x used here, which is therefore predicted to be the high-temperature limit of x in both structure types. However, the difference between maximum and minimum configurational entropy is almost three times larger for spinel than for the TTB structure. This is justified by the fact that a normal spinel ($x = 0$) can be defined as having zero configurational entropy, as both sublattices are fully occupied by only one cation. For the TTB structure, on the other hand, there is always a mixed occupancy between cations and vacancies on at least one of the sublattices, and so the configurational entropy is never zero. This means that there is less driving force for disordering for the TTB structure than for spinels, and that enthalpic effects can be expected to dominate the tungsten-bronze-type oxides also at higher temperatures.

Using α and β obtained above, we calculate the degree of cation interchange, x in (1), as a function of temperature. The result is plotted in Figure 6, which also gives the temperature dependence of α and β (inset panel). For BN, both α and β are very

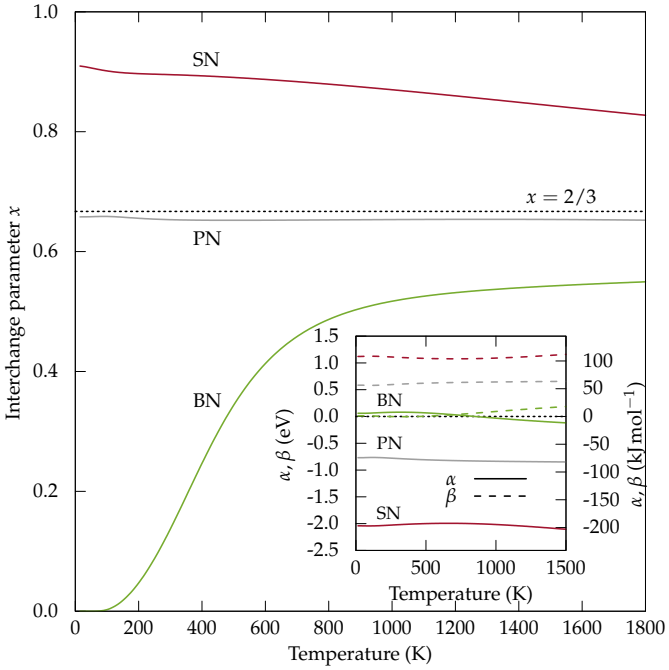

Fig. 6 Degree of cation interchange as a function of temperature for BN, SN and PN, calculated from Equation (3). The high-temperature limit $x = 2/3$, corresponding to maximal configurational entropy, is marked with a dotted black line. Inset plot shows the temperature dependency of the fitting parameters α (solid lines) and β (dashed).

small, which means that entropy is the main factor that governs

the degree of cation inversion. BN therefore has a prominent temperature dependency, while both PN and SN, which have much more distinct minima in enthalpy (Figure 5a), show only a weak dependency of x on temperature (Figure 6). As is also the case for spinels,[16] α and β are of similar magnitude, but with opposite sign (inset of Figure 6).

4 Discussion

4.1 Possibility of cation ordering in tungsten-bronze-type oxides

As Figure 3a shows, the energy differences between different cation configurations are quite small, with a maximal difference of 1.32 eV per unit cell (0.263 eV or 25.4 kJ mol^{-1} per formula unit) for fully relaxed SN, and less for the other compositions. This is somewhat unexpected, as Ba^{2+} is significantly larger than Sr^{2+} and Pb^{2+}, so especially the PP configurations, with more cations in the narrow square channels, would be expected to lie high in energy for BN. This is the case for the initial structures (blue bars in Figure 2a–c), where two of the SS configurations have a much lower energy than the others, as expected from atomic size considerations. After relaxation of the structure is taken into account, the energy landscape is relatively flat, with energy differences smaller for BN than for both SN and PN. The main contribution to this energy landscape flattening comes from the ionic movements (red bars in Figure 2a–c), and only to a lesser extent from volume change (yellow bars). Although the energetic contribution from volume change is larger for BN than for SN and PN, the volume change itself is not systematically larger for BN, as seen in Figure 3b.

The flatness of the energy landscape, particularly for BN, is striking, see Figure 2. This difference in behaviour of BN relative to SN and PN can be rationalized from the relative size of the cations and the coordination environment inside the channels. The square channels are formally 12-coordinated and similar to the A-sites in ABO_3 perovskites. The pentagonal channels are formally 15-coordinated, although in practice both the square and pentagonal coordination polyhedra are to some degree distorted and the effective coordination number is therefore less than the formal value. This distortion of A-site coordination polyhedra happens to a larger degree for Sr^{2+} and less for Ba^{2+}, since Sr^{2+} is significantly smaller than Ba^{2+} (ionic radii of 1.58 Å and 1.74 Å, respectively, when extrapolating Shannon values[34] to CN = 15). Sr^{2+} therefore has higher ability to shift towards an off-centered position in the channel, thus obtaining a smaller effective coordination number than Ba^{2+}. This enhanced ability to off-center and distort the structure enables the SN configurations to relax further towards their local energy minima than BN, where full relaxation is partially restricted by the large Ba^{2+} ions. In the case of Pb^{2+}, additional contributions may result from covalent bonding between Pb and O.

Although the energy differences shown in Figure 3a are small, the transition barriers between configurations are large, on the order of 1.0–2.5 eV. This is far above the thermal energy at synthesis conditions, which is on the order of 0.1–0.2 eV. We have only looked at transitions corresponding to diffusion within the square or pentagonal channels, i.e., transitions that do not change the value of x. We expect that since the channel cross-sections are larger than the openings between the channels, transitions that change x will have even higher barriers than those investigated at present.

Although our zero-kelvin DFT calculations indicate that the structure is not able to explore its entire configurational space, the situation might be very different at higher temperatures. During cooling from synthesis temperatures of typically 1300–1400 °C, it is possible that certain configurations are "frozen in" and persist to lower temperatures, where the different local space group symmetries (some of which are polar, cf. Table 1) can aid in the nucleation of the ferroelectric phase. This is similar to the scheme suggested for the lead-free perovskite relaxors studied by Gröting *et al.*,[19] where it was concluded that the small energy differences between different A-site configurations are not sufficient to create long-range order, but that short-range ordering may still be possible. Locally ordered regions that freeze in at high temperature in the paraelectric state, will most likely influence the nature of the ferroelectric ground state. For example, the relatively flat energy landscape predicted for BN might allow more of a long-range cooperativity in the ferroelectric phase, while the larger energetic differences between configurations of SN could lead to less long-range ordering in the ferroelectric state. This could in turn be an explanation for the tendency for SBN materials to become more relaxor-like for Sr-rich compositions. For PN, although more similar to SN in terms of energetics and cation radius, we expect the stereochemically active $6s^2$ lone pair on Pb^{2+} to play a significant role in the ferroelectric transition, and this might trump the contribution from energetics which would otherwise have made the material more similar to SN.

The volume change shown in Figure 3b is, in effect, the ΔV associated with reaction (1). Volume change for order–disorder processes has been addressed previously in the case of spinels.[35] In general, the order–disorder volume $\Delta V = V_{\text{disorder}} - V_{\text{order}}$ for spinels can be positive or negative, but more often positive, and largest (up to 5 %) when the disordering process involves changes in coordination numbers of the cations. Largely normal spinels such as $MgAl_2O_4$ tend to become more inverse with increasing pressure, and it has been observed that this compound disorders more with temperature under high-pressure conditions.[35,36] However, at ambient temperature, high pressure alone has only a negligible effect on the cation distribution,[37] which is also one of the assumptions in the thermodynamic model employed in this work.

4.2 Analogy to spinels and adaptation of O'Neill–Navrotsky model

As stated in the introduction, it should be possible to exploit the similarities between TTB's and spinels in the phenomenological analysis of order–disorder processes. A central question in this respect concerns the transferability of the O'Neill–Navrotsky model. First, it is assumed that non-configurational contributions to the entropy of reaction (1) are negligible. This works well for the interchange process in spinels, and we have made the same as-

sumption here. In addition to the configurational entropy, there could in principle be a contribution from change in vibrational entropy. Since the cation configurations differ with respect to local space group symmetry (Table 1), the number of vibrational modes will also be different, with more modes for configurations of lower symmetry. We do not attempt here to explicitly include this presumably small entropy contribution in the thermodynamic model.

Accepting the premise of configurational entropy only, the conceptually most important difference between TTB's and spinels is revealed by the entropy plot shown in Figure 5b: Since at least one of the sublattices in TTB has a mixed occupancy for all x, the configurational entropy is never zero. In other words, there is no value of x for which the structure must necessarily be fully ordered. This is in contrast to spinels, where a normal spinel ($x = 0$) *must* be perfectly ordered, while an inverse spinel ($x = 1$) can be either ordered or disordered, depending on how the A and B cations distribute over the octahedral sites (the latter is not given by the value of x). Even a "random" spinel ($x = 2/3$) can have different degrees of order, even though the configurational entropy is at a maximum for this degree of inversion. For TTB's, however, any degree of inversion can have varying degrees of order, so there is no *a priori* reason for $x = 0$ to be defined as the ground state.

In light of the above considerations, it is clear that x in itself is not a measure of the degree of disorder, but should merely be though of as a parameter describing the distribution of cations between two sublattices. Order–disorder can take place on each of these sublattices. In a spinel, a transition from normal to (partially or completely) inverse, must necessarily be accompanied by disorder, and so it is expected that the parameter α always be positive for spinels. This is indeed found to be the case,[16,38] so the negative values obtained for α for the TTB materials (inset of Figure 6) may seem counter-intuitive when compared to α values for spinels. However, once it is realized that reaction (1) is not in itself a disordering process, a negative α is not problematic: It merely reflects the fact that a cation interchange from the SS configurations towards the SP (and possibly PP) configurations is energetically favoured — to a large degree for SN; to a somewhat lesser degree for PN; and for BN, the flat energy landscape is reflected in the very small values of α and β.

Turning to the plot of x as a function of temperature (Figure 6), the different behaviour of BN, SN and PN can be understood in light of the above considerations. For BN, x increases with temperature, since the lowest-energy configuration at zero temperature has $x = 0$. The contribution from configurational entropy acts to push the structure towards a higher degree of cation interchange at higher temperature, similar to the behaviour of normal spinels. As the energy landscape for BN is so flat, the effect of entropy is large, and x rapidly approaches $2/3$ when the temperature increases. For SN, however, the energy differences between the configurations are much larger, with a pronounced enthalpy minimum at around $x = 0.9$, which does not change significantly with temperature, as shown in Figure 5a. The effect of increased temperature is therefore to push x towards a slightly lower value, giving the behaviour of decreasing x shown for SN in Figure 6. PN is intermediate between BN and SN in terms of how deep the enthalpy minimum is (Figure 5), but as this minimum is located at around $x = 0.65$, very close to the high-temperature limit of $x = 2/3$, the temperature dependence of x becomes extremely weak for this compound, resulting in the almost flat curve for PN in Figure 6.

The use of a thermodynamic model provides a more complete picture of the behaviour of BN, SN and PN at realistic temperatures, as compared to simply calculating the zero-kelvin energy of the different configurations. It should be kept in mind that the transition barriers between configurations are high. The development of x with temperature (Figure 6) represents the true equilibrium state, while in reality the relaxation time for cation ordering will increase exponentially upon reduction of temperature, and a certain configuration will eventually freeze in, as has also been shown for spinels.[38] The main finding is that the preferred value of x differs significantly for BN and SN, which is likely connected to the gradual change in dielectric and ferroelectric properties with changing Sr/Ba-ratio in the SBN system. The strong temperature dependence of x for Ba suggests that changes in the cation configuration due to thermal history is most likely to occur at high Ba content.

In this study, we have only sampled three different values of x, namely 0 (the SS configurations), 0.5 (SP) and 1 (PP), *via* a total of 10 configurations. These are all the possibilities accessible using a 1x1x2 supercell, while a larger supercell would make it possible to sample more of configurational space (*e.g.*, a 1x1x3 supercell would give access to configurations with $x = 0.33$ and $x = 0.67$, as well as more configurations with $x = 0$ and $x = 1$). However, already when using a 1x1x2 supercell, we see a substantial variation of the energies between different configurations of the same x value, and a sampling of more x values would not necessarily improve significantly on the model. At the same time, an advantage of larger supercells would be to remove artifacts from the periodic boundary conditions. The supercells used here contain two octahedral layers, and therefore have a repeat distance of nearly 8 Å along the shortest dimension (the c axis). Larger cells would be advantageous to eliminate all artificial ordering of vacancies, although it is not known if this contribution is significant. In any case, larger supercells would lead to many more configurations to investigate, and also make each configuration significantly more computationally demanding.

5 Conclusion

The energetics of cation ordering in oxides with tetragonal tungsten bronze (TTB) oxides has been investigated by *ab initio* DFT calculations. It is found that different degrees of cation interchange between the A1 and A2 sublattices are preferred for the TTB metaniobates of barium, strontium and lead. Furthermore, a thermodynamic model has been developed for the phenomenology of cation interchange in TTB oxides, based on the model developed for spinels by O'Neill and Navrotsky. Due to the relatively small energy differences between several of the configurations, there is little driving force for long-range cation ordering. For barium metaniobate, the configurational energy landscape is very flat, and a certain temperature dependence of the cation ordering

is to be expected. Due to quite high barriers for transitions between different configurations, we suggest that certain configurations will be "frozen in" during synthesis, and that different local configurations, some of which lead to polar space group symmetries, can act as seeds for nucleation of the ferroelectric phase below T_C.

6 Acknowledgements

The Research Council of Norway (NFR project no. 209337) and The Faculty of Natural Sciences and Technology, Norwegian University of Science and Technology (NTNU) are acknowledged for financial support. Computational resources were provided by NOTUR (The Norwegian Metacenter for High Performance Computing) through the project NN9264K. Sandra Helen Skjærvø (NTNU), Ulrich Aschauer and Nicola A. Spaldin (ETH Zurich) are acknowledged for insightful discussions.

References

1 M. E. Lines and A. M. Glass, *Principles and applications of ferroelectrics and related materials*, Oxford University Press, New York, 2001.
2 G. Goodman, *J. Am. Ceram. Soc.*, 1953, **36**, 368–372.
3 M. H. Francombe, *Acta Crystallogr.*, 1956, **9**, 683–684.
4 M. G. Sahini, T. Grande, B. Fraygola, A. Biancoli, D. Damjanovic and N. Setter, *J. Am. Ceram. Soc.*, 2014, **97**, 220–227.
5 G. H. Olsen, M. H. Sørby, B. C. Hauback, S. M. Selbach and T. Grande, *Inorg. Chem.*, 2014, **53**, 9715–9721.
6 P. B. Jamieson, S. C. Abrahams and J. L. Bernstein, *J. Chem. Phys.*, 1968, **48**, 5048–5057.
7 A. A. Ballman and H. Brown, *J. Cryst. Growth*, 1967, **1**, 311–314.
8 M. Lundberg and M. Sundberg, *J. Solid State Chem.*, 1986, **63**, 216–230.
9 F. Madaro, R. Sæterli, J. R. Tolchard, M.-A. Einarsrud, R. Holmestad and T. Grande, *CrystEngComm*, 2011, **13**, 1304–1313.
10 A. M. Glass, *J. Appl. Phys.*, 1969, **40**, 4699–4713.
11 M. H. Francombe and B. Lewis, *Acta Crystallogr.*, 1958, **11**, 696–703.
12 P. Labbé, M. Frey, B. Raveau and J. C. Monier, *Acta Crystallogr. B*, 1977, **33**, 2201–2212.
13 R. Cohen, *Nature*, 1992, **358**, 136–138.
14 H. Schmalzried, *Z. Phys. Chem.*, 1961, **28**, 203–219.
15 A. Navrotsky and O. J. Kleppa, *J. Inorg. Nucl. Chem.*, 1967, **29**, 2701–2714.
16 H. O'Neill and A. Navrotsky, *Am. Mineral.*, 1983, **68**, 181–194.
17 H. O'Neill and A. Navrotsky, *Am. Mineral.*, 1984, **69**, 733–753.
18 S. Podlozhenov, H. A. Graetsch, J. Schneider, M. Ulex, M. Wöhlecke and K. Betzler, *Acta Crystallogr. B*, 2006, **62**, 960–965.
19 M. Gröting, S. Hayn and K. Albe, *J. Solid State Chem.*, 2011, **184**, 2041–2046.
20 M. Gröting and K. Albe, *J. Solid State Chem.*, 2014, **213**, 138–144.
21 K. Momma and F. Izumi, *J. Appl. Crystallogr.*, 2011, **44**, 1272–1276.
22 H. T. Stokes and D. M. Hatch, *J. Appl. Crystallogr.*, 2005, **38**, 237–238.
23 C. Capillas, E. S. Tasci, G. de la Flor, D. Orobengoa, J. M. Perez-Mato and M. I. Aroyo, *Z. Kristallogr.*, 2011, **226**, 186–196.
24 G. Kresse and J. Hafner, *Phys. Rev. B*, 1993, **47**, 558–561.
25 G. Kresse and J. Hafner, *Phys. Rev. B*, 1994, **49**, 14251–14269.
26 G. Kresse and J. Furthmüller, *Comp. Mater. Sci.*, 1996, **6**, 15–50.
27 G. Kresse and J. Furthmüller, *Phys. Rev. B*, 1996, **54**, 11169–11186.
28 J. P. Perdew, A. Ruzsinszky, G. I. Csonka, O. A. Vydrov, G. E. Scuseria, L. A. Constantin, X. Zhou and K. Burke, *Phys. Rev. Lett.*, 2008, **100**, 136406–136406.
29 P. E. Blöchl, *Phys. Rev. B*, 1994, **50**, 17953–17979.
30 G. Kresse and D. Joubert, *Phys. Rev. B*, 1999, **59**, 11–19.
31 H. J. Monkhorst and J. D. Pack, *Phys. Rev. B*, 1976, **13**, 5188–5192.
32 G. Henkelman, B. P. Uberuaga and H. Jónsson, *J. Chem. Phys.*, 2000, **113**, 9901–9904.
33 G. Henkelman and H. Jónsson, *J. Chem. Phys.*, 2000, **113**, 9978–9985.
34 R. D. Shannon, *Acta Crystallogr. A*, 1976, **32**, 751–767.
35 R. M. Hazen and A. Navrotsky, *Am. Mineral.*, 1996, **81**, 1021–1035.
36 F. Meducin, S. a. T. Redfern, Y. Le Godec, H. J. Stone, M. G. Tucker, M. T. Dove and W. G. Marshall, *Am. Mineral.*, 2004, **89**, 981–986.
37 F. Nestola, T. B. Ballaran, T. Balic-Zunic, F. Princivalle, L. Secco and A. Dal Negro, *Am. Mineral.*, 2007, **92**, 1838–1843.
38 S. A. T. Redfern, R. J. Harrison, H. S. C. O'Neill and D. R. R. Wood, *Am. Mineral.*, 1999, **84**, 299–310.